

Maximum Startup Capacitance Characteristics of High-power-density Direct-current Power Converters

Chien-Chi Chiu,¹ Tung-Ming Liang,¹ Ming-Tsung Yeh,^{2*} and Yi-Nung Chung¹

¹Department of Electrical Engineering, National Changhua University of Education,
No. 1, Jinde Rd., Changhua City, Changhua County 50007, Taiwan

²Department of Electrical Engineering, National Chin-Yi University of Technology,
57, Sec. 2, Zhongshan Rd., Taiping Dist., Taichung 411030, Taiwan

(Received December 18, 2023; accepted June 11, 2024)

Keywords: analysis for DC power converters, maximum startup capacitance, DC power module characteristics

Direct-current (DC) power converters play an indispensable and crucial role in various systems, particularly in today's increasing electrification of global energy. The characteristics of DC power converters have garnered widespread attention in the design and practical application of energy-saving systems. General system design not only considers the output voltage and power rating of DC power converters but also factors such as efficiency, input voltage regulation, output load regulation, dynamic load regulation, and ripple voltage characteristics as specified in the manufacturer's datasheet. The objective is to provide a stable power supply to ensure the regular operation of the system. However, the characteristics of maximum startup capacitance are often overlooked, and sometimes only numerical values from the datasheet are used as reference, limiting the insight into the startup characteristics curve. The improper assessment of the startup capacitance characteristics may lead to power startup failure or repetitive oscillations, thereby affecting the operational stability of the system. In this study, the in-depth examination of four high-power-density DC power converters is investigated. Firstly, foundational characteristics testing research is conducted. The characteristics of the maximum startup capacitance are examined in this study by constructing and analyzing the experimental environment. In this research, we explain the critical points in constructing the environment for maximum capacitor load testing and compare the differences between passive components for load and electronic load machine simulation experiments. Finally, we complete the experiment in a low-cost detection environment constructed with essential passive components and obtain the maximum capacitor load characteristic curves of the high-power-density DC power converters. This information will become a reference for system design, ensuring the stability assessment of DC power converters under maximum capacitor load conditions. Additionally, sensor integration for real-time performance monitoring further enhances the understanding of startup capacitance dynamics in high-power-density DC power converters.

*Corresponding author: e-mail: mtyeh@ncut.edu.tw
<https://doi.org/10.18494/SAM4835>

1. Introduction

With the advancement of time and technology, we have transitioned from a non-electronic era to the era of smart (consumer) electronics, where electronic products are omnipresent in our daily lives. In this transformation, power supply has consistently played a crucial role in supplying and converting terminal electrical energy. Despite the maturity of the power supply industry, it continues to exert a profound impact on market development.^(1,2)

As shown in Table 1, amid the trend of global economic growth, the emergence of new application markets, such as healthcare, industrial automation, 5G base stations, and data centers, is driving the development of the global power supply market. This indicates that the power supply industry, in response to emerging application demands, continually adapts and propels the market forward, demonstrating its ability to meet evolving needs.^(3–6)

The proliferation of electronic products has brought tremendous convenience to our lives, driving the flourishing development of various electronics and electrical industries. However, it has also triggered significant changes in the realm of electrical power energy. Taking integrated circuits as an example, efforts to achieve greater energy efficiency have led to reduced power supply voltages.^(7,8) Furthermore, efficiency has been enhanced in the process of miniaturizing direct-current (DC) power converters, accompanied by excellent thermal loss characteristics. This trend indicates that energy consumption will become a crucial design consideration in the system and circuit design stages.⁽⁹⁾

2. Data, Materials, and Methods

With the trend towards the miniaturization of electronic products, switched-mode DC power converters play a crucial role in system design. In the system engineering design phase, in addition to essential parameters such as input voltage, output voltage, and output current, there are also startup voltage response, output current response, input voltage regulation, ripple voltage, load regulation, load transient response, maximum capacitor load characteristics,

Table 1
Power supply application overview statistics.

	(AC–DC) Power converter	(DC–DC) Power converter
Data center	V	V
Communication equipment	V	V
Industrial sector	V	V
Defense/aerospace domain	V	V
Medical field	V	V
Office desktop computing system	V	
Portable device charger	V	
Consumer goods	V	

Source of information: Industrial Technology Research Institute Industry Economics and Knowledge Consulting (ITRI IEK)
V: suitable for application areas

efficiency, and more. These conditions play a vital role in system design, and hence, it must be ensured that switched-mode DC power converters operate stably in various scenarios.^(10,11)

System developers typically refer to the original manufacturer's specification sheets or testing documents corresponding to the specific brand and model of the equipment to understand the DC power converter's performance and quality characteristics. In these documents, dynamic data demonstrating the internal control characteristics of the switched DC power converter are particularly important. These include startup voltage response, output current response, load transient response, and maximum capacitor load capacity.^(12–15) Among these data, the waveform curve of the maximum capacitor load capacity is a crucial indicator for evaluating the soft-start capability of a switched-mode DC power converter. Unfortunately, it is currently impossible to obtain detailed evaluations of this test waveform from the information provided by the original manufacturer.

For testing, we select DC–DC power converters produced by internationally renowned manufacturers. A testing process and environment based on the specifications and test reports provided by the original equipment manufacturer (OEM) are established in this study. During the setup of the testing and verification environment, test methods are adjusted to enhance accuracy. The testing environment's effectiveness is confirmed by comparing the actual test results with the data in the OEM test documents. Using the established testing environment, waveform curves of the maximum capacitor load characteristics for each module can be obtained, providing a more valuable power converter characteristic analysis for system development. Such research can improve system development efficiency and ensure power converter stability in various application scenarios.

2.1 Equipment under test

The selected DC power converters shown in Table 2 are commercially available products with a specified rating of 48 V isolation, chosen as the test subjects for this research. In establishing the relevant testing techniques and environment, we referred to the specifications of these converters. The specifications include an input of DC 48 V, stepping down to outputs of 5 V, 20 A, and 100 W, and an efficiency greater than or equal to 90%, among other relevant conditions. We considered the potential for measurement errors during the setup of the testing environment, ensuring that the experimental references met technical thresholds and measurement accuracy to guarantee the accuracy of the results. Throughout the experimental process, we compared our conditions and specifications with those provided by the OEM to confirm whether the empirical references align with technical standards.^(16–21)





2.2 Experimental setup and analysis

2.2.1 Efficiency measurement environment construction and measurement results

Efficiency measurement typically involves calculating the ratio of output power to input power. This can be achieved by multiplying the output voltage and output current, then dividing

Table 2

(Color online) Power supply application overview statistics of tested DC power converters.

	Artesyn	COSEL	DELTA	MuRata
Model	AVD100-48S05-6L	CHS1204805	V48SH05020NNFA	ULS-5/20-D48NM-C
Exterior				
V_{in} (V)	36–75	36–76	36–75	36–75
V_{out} (V)	5	5	5	5
I_{out} (A)	20	24	20	20
Watts (W)	100	120	100	100
Efficiency (%)	92.5	93	91.5	91
Ripple noise (mV _{p-p})	120	150	160	120
Start-up time (ms)	N/A	50	28	20
Dynamic load response (mV _{p-p})	600	600	320	480

them by the input voltage and input current product. However, during such measurement, it is essential to consider the impedance characteristics of the measurement cables to ensure accuracy. The detailed measurement method can be seen in Fig. 1. In this process, the impedance characteristics of the cables can affect the efficiency measurement. Therefore, experimental design requires special attention to obtain reliable efficiency data.

By comparing the measurement results in Table 3, we confirmed that the data obtained in the established verification environment aligns with the OEM's efficiency specification curve, with the error falling within an acceptable range. The efficiency performance under light and full loads may vary because of the diverse design structures of different power converters. Generally, efficiency peaks often occur in the range of 40 to 80% load, which aligns well with the principles and considerations of system design.

2.2.2 Ripple voltage measurement environment construction and measurement results

Because of the periodic switching of MOSFETs through pulse-width modulation in switched-mode power supplies to achieve a stable output, this operation generates high-frequency ripples in the output voltage. These ripples superimpose on the DC output voltage, causing unnecessary interference in the system. Therefore, measuring the ripple voltage of a DC power converter is one of the essential tasks in confirming its performance.

The ripple voltage measurement environment setup is shown in Fig. 2. The measured signals are relatively small voltage signals, so they are susceptible to external test environmental effects that may cause noise and potential measurement errors. To mitigate such issues, oscilloscope probe settings are typically configured with a bandwidth of 20 MHz for acquisition. The probes are shorted to ground to minimize the coupling of spurious interference. This configuration aids in more accurately measuring the waveform of the primary ripple (refer to Fig. 3 for details of the measurement setup).

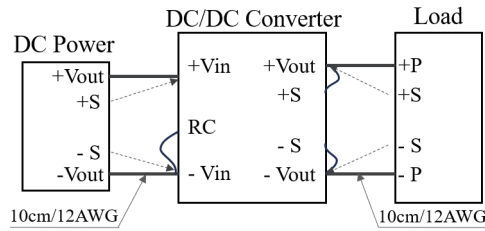


Fig. 1. (Color online) Schematic diagram of efficiency curve measurement environment.

Table 3
Efficiency measurement test data analysis results.

Company	Sample serial number	$V_{in} = 38\text{ V}$			$V_{in} = 48\text{ V}$			$V_{in} = 57\text{ V}$			Original specifications
		$I_{out} = 0\text{--}20\text{ A}$			$I_{out} = 0\text{--}20\text{ A}$			$I_{out} = 0\text{--}20\text{ A}$			
		2 A	10 A	20 A	2 A	10 A	20 A	2 A	10 A	20 A	
Artesyn	1	86.965	93.836	91.814	83.937	93.137	92.286	82.796	91.521	91.974	92.5%
	2	86.429	93.897	91.460	86.468	93.441	91.460	82.210	91.930	91.330	
	3	86.781	93.636	91.597	86.606	92.948	92.091	82.630	92.304	91.294	
COSEL	1	86.778	94.314	93.267	83.300	93.795	92.928	78.889	92.313	92.769	93%
	2	86.894	94.426	93.378	83.370	93.861	92.999	78.977	92.396	92.878	
	3	86.960	94.499	93.109	83.491	93.156	92.705	79.068	92.493	92.463	
DELTA	190600704	81.427	92.402	90.613	80.127	92.199	90.858	78.942	91.415	90.816	91.5%
	190600722	81.140	92.073	90.334	79.900	91.109	90.598	78.672	91.097	90.489	
	190600723	81.200	92.138	90.412	79.898	91.140	90.620	78.694	91.134	90.561	
MuRata	1566B920C	86.531	92.699	89.808	86.541	91.895	90.266	86.530	91.075	89.650	91%
	1180B920C	86.255	93.079	89.837	86.260	92.413	89.616	86.266	91.760	89.392	
	1561B920C	86.763	92.939	89.961	86.733	92.094	90.031	82.651	91.318	89.815	

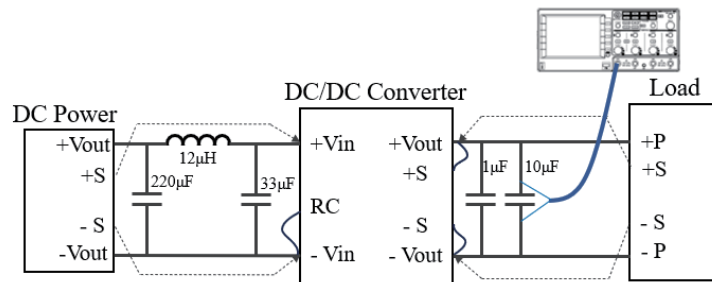


Fig. 2. (Color online) Schematic diagram of ripple voltage measurement environment.

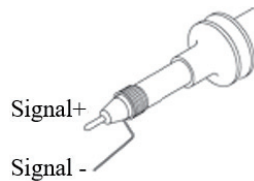


Fig. 3. Schematic diagram of oscilloscope probe short grounding method.

According to the measurement results in Table 4, COSEL exhibits the minimum output ripple voltage among the four purchased commercial power converters after actual testing. Under full load, the ripple voltages of Artesyn and MuRata are relatively close, but under no-load conditions, Artesyn's ripple voltage surpasses that of MuRata. The experimental data for Delta's output ripple voltage show a significantly larger peak-to-peak voltage than those of the three aforementioned power converter modules. After confirming the oscilloscope probe grounding and setup and comparing the testing procedures with the other three power converters, it is ultimately determined that the test data are accurate and agree with the reference values.

2.2.3 Load variation response measurement environment construction and measurement results

According to the load variation response test method depicted in Fig. 4, the procedure begins by fixing the input voltage. Subsequently, the output current of the power converter is switched from 25 to 50% of the rated load, followed by another switch to 75% of the output current. An

Table 4
Output ripple voltage measurement test data analysis results.

Company	Sample serial number	Ripple and noise 0 A_Load	Ripple and noise 20 A_Load	Original specifications
		Output C = 1 μ F 10 μ F Input CLC = 220 μ F-12 μ H-33 μ F	Output C = 1 μ F 10 μ F Input CLC = 220 μ F-12 μ H-33 μ F	
Artesyn	1	48 mV	78 mV	120 mV
	2	45 mV	74 mV	
	3	48 mV	74 mV	
COSEL	1	33 mV	42 mV	150 mV
	2	37 mV	43 mV	
	3	36 mV	42 mV	
DELTA	190600704	107 mV	119 mV	160 mV
	190600722	108 mV	115 mV	
	190600723	110 mV	120 mV	
MuRata	1566B920C	62 mV	74 mV	120 mV
	1180B920C	61 mV	75 mV	
	1561B920C	58 mV	73 mV	

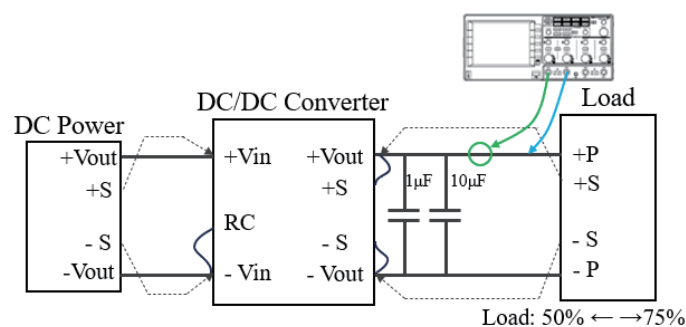


Fig. 4. (Color online) Schematic diagram of load change response measurement environment.

electronic load machine performs this series of operations continuously and automatically. During the test, the discharge capability of the electronic load machine is set to a maximum discharge rate of $2.5 \text{ A}/\mu\text{s}$, with a discharge duration set at $500 \mu\text{s}$ and a time interval of $500 \mu\text{s}$ between switches. The changes in current are observed using a current probe while simultaneously monitoring the range of voltage fluctuations to assess the system's response during load variations.

To observe the load variation response time, the measurement is conducted during the load variation scenario, switching the output from 50 to 75% of the current. The sampling time range is based on the condition of $(1/e, \Delta V_{out} = 37\%)$, that is, from the beginning of the switch until the voltage change reaches 37%. Details of time range sampling can be gleaned from Fig. 5. This approach effectively evaluates the system's rapid response to load variations.

According to the conclusions drawn from the load variation response test, as shown in Table 5, the MuRata power converter performs the best among the four purchased DC power converters. In its dynamic response characteristics, the average overshoot of the output voltage is below 280 mV and the average response time to load variation is less than $11 \mu\text{s}$, with some oscillation voltage present in the response waveform. The Artesyn power converter follows, with

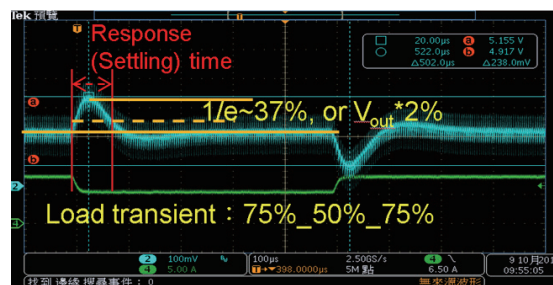


Fig. 5. (Color online) Load response time waveform measurement.

Table 5

Load change response measurement test data analysis results.

$V_{in} = 48 \text{ V}$, Current transient LO = 75%-50%-75%, Output C = $1 \mu\text{F} 10 \mu\text{F}$, $T_a = +23-25 \text{ }^\circ\text{C}$					
Company	Sample serial number	Load change spike (mV _{p-p})	Original specifications	Voltage spike drop to 37% ((mV _{p-p} /2)*37%)	$\Delta V = 37\%$ Response time
Artesyn	1	344 mV	N.A.	64 mV	15 μs
	2	343 mV		64 mV	13 μs
	3	342 mV		64 mV	13 μs
COSEL	1	388 mV	N.A.	72 mV	15 μs
	2	389 mV		72 mV	14 μs
	3	368 mV		68 mV	16 μs
DELTA	190600704	518 mV	320mV	96 mV	16 μs
	190600722	498 mV		92 mV	16 μs
	190600723	497 mV		92 mV	16 μs
MuRata	1180B920C	279 mV	480mV	52 mV	12 μs
	1566B920C	280 mV		52 mV	11 μs
	1561B920C	249 mV		46 mV	8 μs

an average overshoot of the output voltage below 350 mV, an average response time to load variation of less than 14 μs , and a minimal oscillation voltage in the response waveform. The characteristics of the COSEL power converter are slightly inferior to those of the first two, with an average overshoot of the output voltage below 382 mV, an average response time to load variation of less than 15 μs , and a more notable oscillation voltage in the response waveform. Finally, the Delta power converter exhibits poorer characteristics in these aspects, with an average overshoot of the output voltage below 498 mV, an average response time to load variation of less than 16 μs , and an oscillation voltage in the response waveform.

2.2.4 Start response measurement environment construction and measurement results

According to the setup of the startup response test environment shown in Fig. 6, the main steps include fixing the input voltage and providing the corresponding current while simultaneously fixing the discharge current at the load end. By changing the switch state of the power supply, the time required for the startup of the DC power converter is observed.

According to the startup response test results in Table 6, the COSEL power converter performs the best at the startup speed, with an approximate output voltage startup delay of 6.1 ms and an output current startup delay of about 10.2 ms. The MuRata power module follows, with an output voltage startup delay of around 10.3 ms and an output current startup delay of approximately 14.7 ms. The performance of the Delta power module is moderate, with an output voltage startup delay of about 13.6 ms and an output current startup delay of around 26.9 ms. The Artesyn power module has an average output time exceeding 50 ms, with an output voltage startup delay of about 52.6 ms and an output current startup delay of approximately 57.8 ms.

2.3 Maximum capacitive load characteristics measurement

The scenario depicted in Fig. 7 illustrates the situation during the startup phase of the power system, where capacitors, owing to their charging and discharging capabilities, may absorb a significant amount of current. This condition can lead to overcurrent during startup, putting stress on power equipment and circuit components. It may even trigger protective devices, causing the system to restart repeatedly.

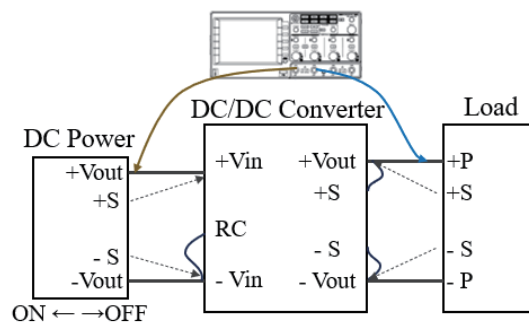


Fig. 6. (Color online) Schematic diagram of startup response measurement environment.

Table 6
Startup response characteristic measurement test data analysis results.

Company	Sample serial number	Power ON	Power ON	Power ON	Original specifications
		Startup Load=0 A Voltage startup delay time	Startup Load=20 A Voltage startup delay time	Startup Load=20 A Current startup delay time	
Artesyn	1	51.8 ms	52.2 ms	57.8 ms	N/A
	2	52.4 ms	52.4 ms	57.4 ms	
	3	52.0 ms	52.6 ms	57.2 ms	
COSEL	1	5.9 ms	6.0 ms	10.1 ms	50 ms
	2	6.0 ms	6.1 ms	10.2 ms	
	3	5.9 ms	6.0 ms	10.2 ms	
DELTA	190600704	13.6 ms	13.7 ms	26.5 ms	28 ms
	190600722	13.6 ms	13.9 ms	26.9 ms	
	190600723	13.5 ms	13.6 ms	26.2 ms	
MuRata	1566B920C	9.7 ms	9.9 ms	14.3 ms	15 ms
	1180B920C	9.5 ms	10.3 ms	14.7 ms	
	1561B920C	9.2 ms	10.1 ms	14.7 ms	

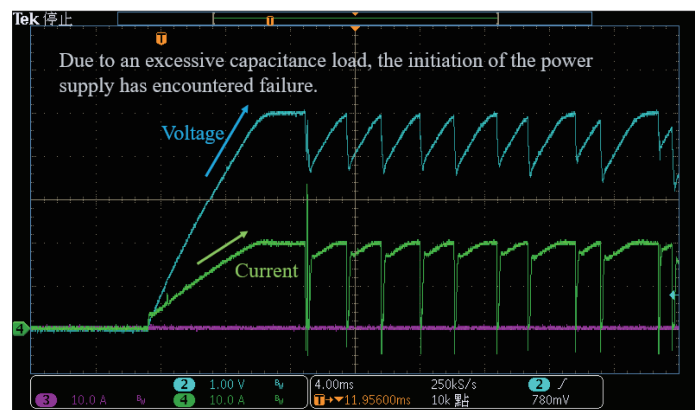


Fig. 7. (Color online) The capacitive load is very large, triggering the protection waveform.

2.3.1 Brief description of maximum capacitive load characteristics

In the maximum capacitor load test, the relationship between various currents is as depicted in Fig. 8. The total current I_S is the sum of I_{CL} and I_{RL} , where I_{RL} is the maximum rated current output of the tested power supply system and I_{CL} represents the current absorbed by the capacitor.

According to the oscilloscope waveform in Fig. 9, the startup voltage is V_S , the total current is I_S , and the capacitor charging characteristics of I_{CL} occur at the startup moment. Based on the performance of the DC power converter, after several time constants, the current reaches the output state of the maximum rated current, at which point, the current is I_{RL} .

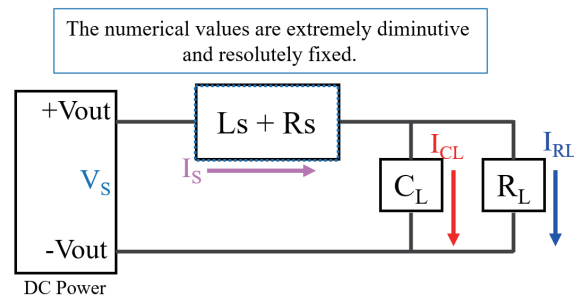


Fig. 8. (Color online) Relationship between total current I_S , capacitor charging current I_{CL} , and load current I_{RL} .

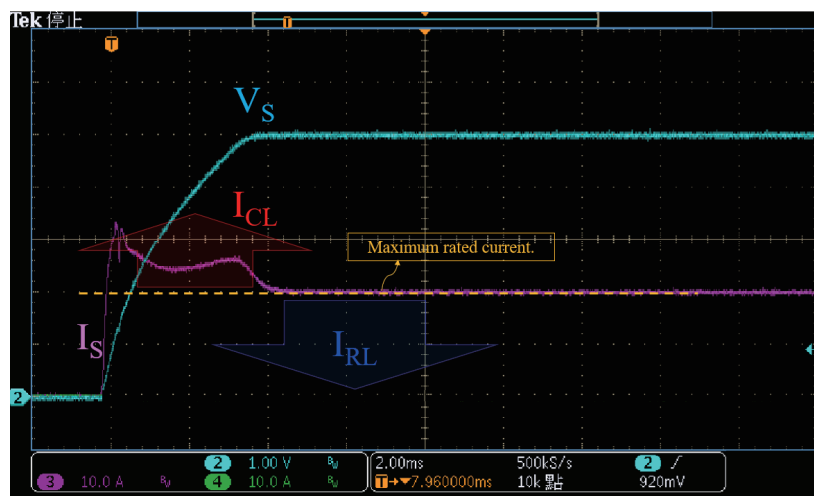


Fig. 9. (Color online) Description of the waveform diagrams of total current I_S , capacitor charging current I_{CL} , and load current I_{RL} .

2.3.2 Some common mistakes

The reason for not being able to use electronic load equipment to simulate R_L is that there may be mutual interference between two or more control systems, which could lead to errors in the experiment. When conducting experiments or testing control systems, additional variations or disturbances may be introduced if multiple control systems affect each other. This situation can result in differences between measured results and expected outcomes, as illustrated in the system architecture in Fig. 10.

As depicted in Fig 11, conducting experiments using electronic load equipment may lead to the phenomenon of cross-interference. When I_{CL} generates a current spike, it is evident that the electronic load device and the DC power converter generate a slow rise in I_{RL} . This indicates that the operation of the backend control system may impact the measurement or results of the frontend control system, potentially causing deviations in the outcomes.

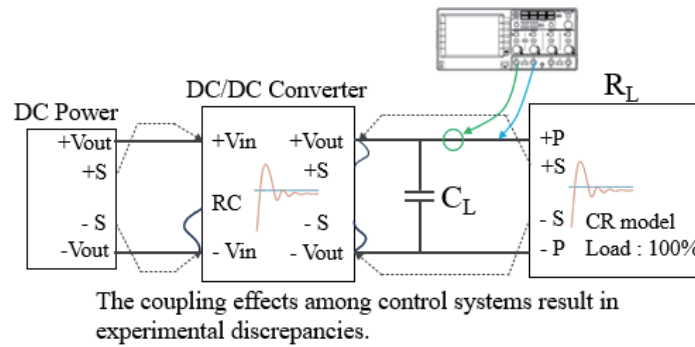


Fig. 10. (Color online) Schematic diagram of R_L experiment simulation using electronic load equipment.

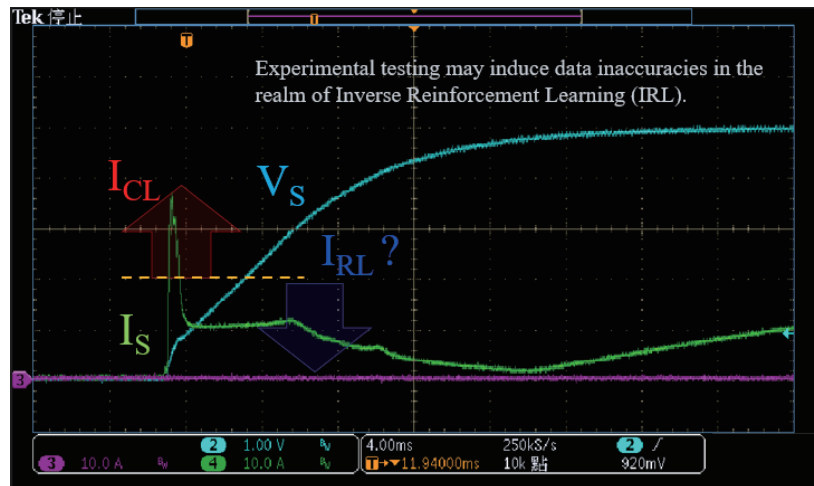


Fig. 11. (Color online) When using an electronic load device to simulate R_L , the test result is a deviated waveform diagram.

2.3.3 Measurement methods used

Based on the experiment and environment setup described above, the measurement environment for the maximum capacitance load test is illustrated in Fig. 12. In this experiment, R_L is tested using passive components and high-power resistors. C_L varies during the investigation, and the voltage and current waveforms of the DC power converter are measured using an oscilloscope. In the measurement process, the oscilloscope probes are set with a bandwidth of 20 MHz and grounded using a short-circuit configuration.

3. Experimental Results and Discussion

The output maximum capacitance load test results for the Artseyn power converter are presented in Fig. 13. In this test, the overcurrent protection range of the Artseyn power converter

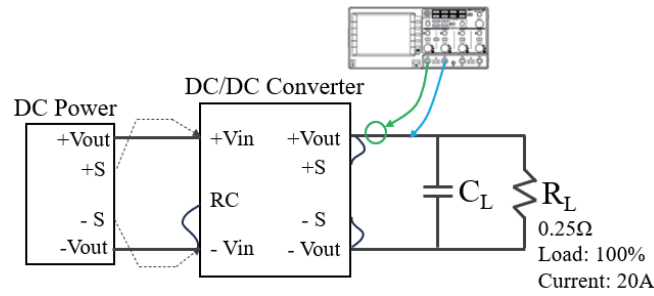


Fig. 12. (Color online) Schematic diagram of the maximum capacitive load measurement environment.

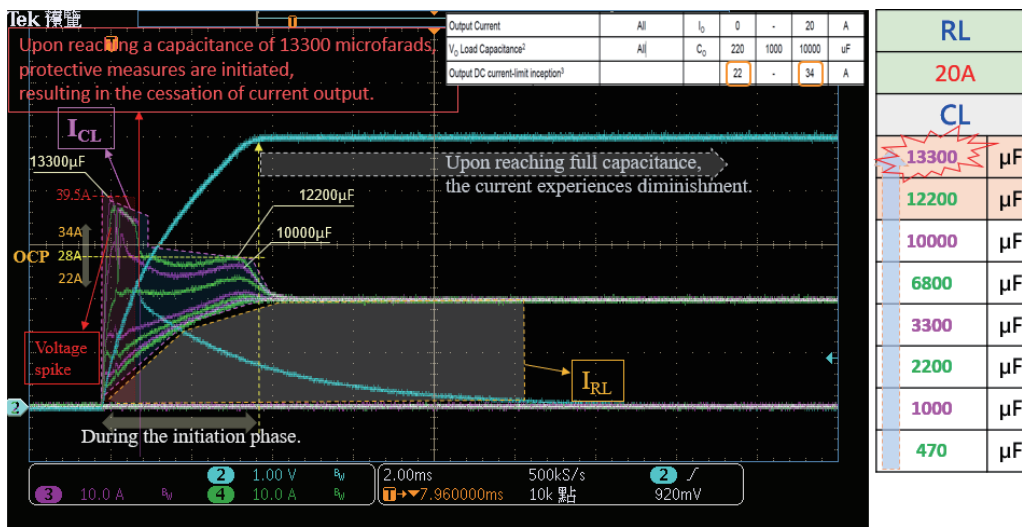


Fig. 13. (Color online) Arytesyn power converter output maximum capacitive load test waveform.

is from 22 to 34 A, with a median value of 28 A. The overcurrent protection is triggered when the load capacitance is 13300 μF , the maximum peak current is 39.5 A, and the duration is less than 2 ms. After comparing the protection waveform with the original specifications, it is determined that the lack of protection action at a load capacitance of 12200 μF might be due to the startup current exceeding the maximum overcurrent of 34 A.

The output maximum capacitance load test results for the COSEL power converter are depicted in Fig. 14. In this test, the overcurrent protection point for the COSEL power converter is located at 1.05 times the upper current limit of 24 A, that is, 25.2 A. However, during the startup transient with a load capacitance above 10000 μF , it consistently exceeds this protection point. Interestingly, no overcurrent protection is observed even with an increase in maximum load capacitance to 33000 μF , with a maximum peak current of 40 A.

The output maximum capacitance load test results for the Delta power converter are illustrated in Fig. 15. In this test, the Delta power converter's overcurrent protection range is between 22 and 28 A, with a midpoint of 25 A. Although the overcurrent protection is not

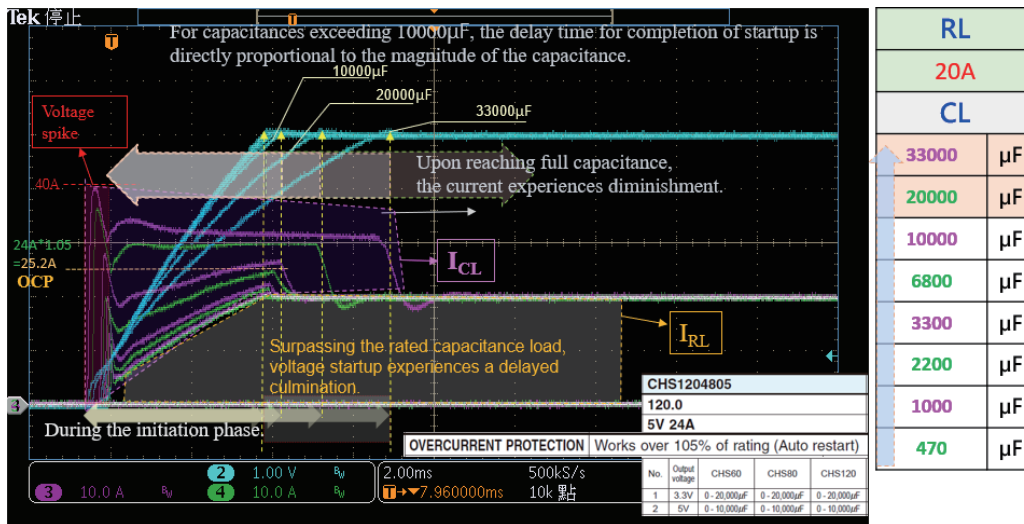


Fig. 14. (Color online) COSEL power converter output maximum capacitive load test waveform.

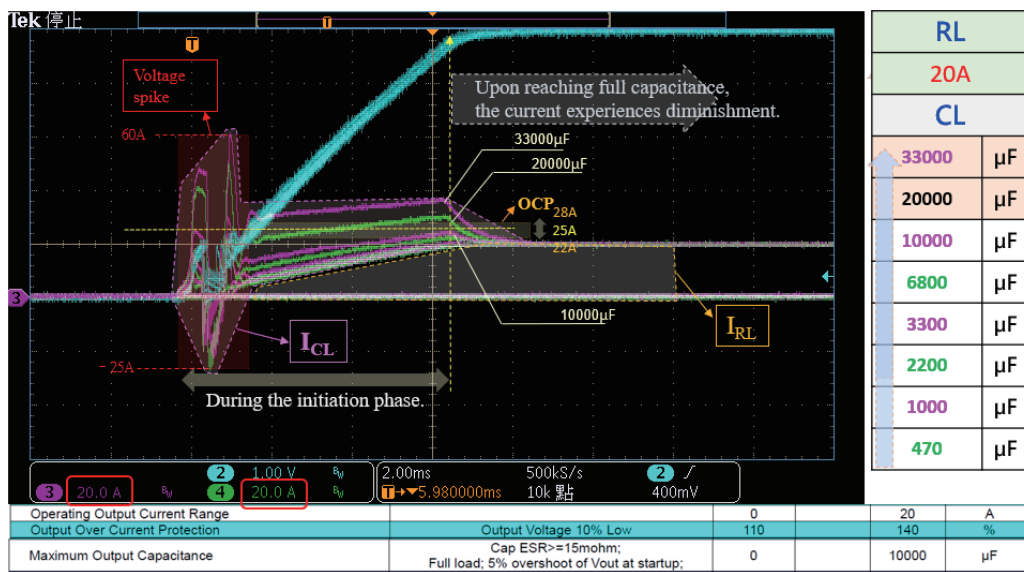


Fig. 15. (Color online) Delta power converter output maximum capacitive load test waveform.

triggered, even with an increase in maximum load capacitance to 33000 μ F, the current waveform deviates from the previous waveform beyond the specified maximum capacitance of 10000 μ F. Eventually, it falls into the overcurrent protection range, reaching a maximum peak current of 60 A. Notably, Delta is the only module in the test where a negative current is observed.

The output maximum capacitance load test results for the MuRata power converter are presented in Fig. 16. In this test, the overcurrent protection range for the MuRata power converter

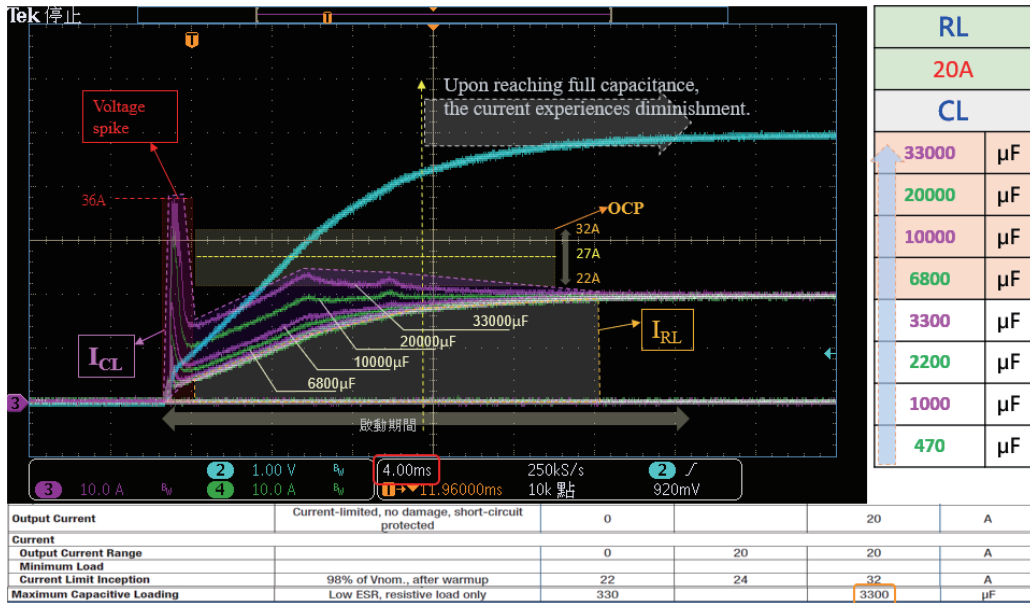


Fig. 16. (Color online) MuRata power converter output maximum capacitive load test waveform.

is between 22 and 32 A, with a midpoint of 27 A. However, overcurrent still occurs without triggering protection when the maximum load capacitance is increased to 33000 μF. The current waveform starts to deviate from the previous waveform beyond the specified maximum capacitance of 3300 μF, reaching a maximum peak current of 36 A. Notably, the MuRata module exhibits good consistency in this test, and the rise time to establish the rising voltage is completed within 20 ms.

4. Conclusions

Four DC power converters with the same specifications (100 W, 48 to 5 V/20 A) were experimentally analyzed in this study. The test environment’s effectiveness was confirmed by comparing the test results with the OEM specifications. With these testing methods and environments, through the integration, comparison, and analysis of results, the waveform diagrams of the maximum capacitor load characteristics for each module were successfully obtained, providing a valuable reference for analyzing the maximum capacitor load characteristics of power converters in system development. With the current lack of commercially available validation platforms, the results of this study offer a valuable reference for system developers in terms of testing methods and characteristic analysis data, which is essential information for design and validation.

References

- 1 ITRI IEK M. J. Huang, IEK Industry Intelligence Network Global Power Supply Market Outlook: https://ieknet.iek.org.tw/iekrpt/rpt_more.aspx?actio1 (accessed December 2022) (in Chinese).
- 2 ITRI IEK W. R. Yang, IEK Industry Information Network Energy Storage Power Converter Technology Development Trends: https://ieknet.iek.org.tw/iekppt/ppt_more.aspx?actiontype=ppt&indu_idno=5&slid_preid=6300 (accessed December 2022) (in Chinese).
- 3 Technology Collaborative Program on High Temperature Superconductivity: <https://www.ieahts.org> (accessed October 2022).
- 4 World Energy Outlook: <http://www.worldenergyoutlook.org/publications/weo-2014/> (accessed October 2022).
- 5 F. Udrea, G. Deboy, and T. Fujihira: IEEE Trans. Electron Devices **64** (2017) 713. <https://doi.org/10.1109/TED.2017.2658344>
- 6 The Edison Foundation Transforming America's Power Industry, The Investment Challenge 2010–2030: https://www.edisonfoundation.net/-/media/Files/IEI/publications/Transforming_Americas_Power_Industry.pdf (accessed October 2022).
- 7 T. Andersson and D. Nilsson: STRI Report, Test and Evaluation of Voltage Dip Immunity (2002) <https://odr.chalmers.se/handle/20.500.12380/165652> (accessed October 2022).
- 8 M. H. Bollen: Understanding Power Quality Problems: Voltage Sags and Interruptions, Wiley-IEEE Press, Eds. (IEEE Press, 2000) 1st ed., Chap.1–3.
- 9 E. Moore and T. Wilson: IEEE Trans. Magn. **2** (1966) 620. <https://doi.org/10.1109/TMAG.1966.1065901>
- 10 M. S. Makowski and D. Maksimovic: Proc. 1995 Power Electronics Specialist Conf. (PESC, 1995) 1215–1221. <https://doi.org/10.1109/PESC.1995.474969>
- 11 Z. Pan, F. Zhang, and F. Z. Peng: Proc. 2005 IEEE Applied Power Electronics Conf. (APEC, 2005) 1393–1398. <https://doi.org/10.1109/APEC.2005.1453209>
- 12 K. D. T. Ngo and R. Webster: Proc. 1992 23rd IEEE Power Electronics Specialists Conf. (PESC, 1992) 378–385. <https://doi.org/10.1109/PESC.1992.254649>
- 13 Texas Instruments Load Dump and Cranking Protection for Automotive Backlight LED Power Supply: https://www.ti.com/lit/an/snva681a/snva681a.pdf?ts=1702784376316&ref_url=https%253A%252F%252Fwww.google.com%252F (accessed October 2022).
- 14 ADI Analog Dialogue Power Supply Management-Principles, Problems, and Parts: <https://www.analog.com/en/analog-dialogue/articles/power-supply-management.html> (accessed October 2022).
- 15 M. D. Seeman, S. R. Sanders, and C. Hall: IEEE Trans. Power Electron. **23** (2008) 841. <https://doi.org/10.1109/TPEL.2007.915182>
- 16 Advanced Energy AVD100-48S05 Series 100 Watts Sixteenth-brick-Converter Technical Reference Note: https://artesycom-prod.scdn8.secure.raxcdn.com/assets/trn_dc_dc_avd100-48s05_release1472721778_techref.pdf?a=c20b9f94c4dfc2aa779372ef1a247b7f49e4ad53 (accessed October 2022).
- 17 COSEL CHS-series Catalog: https://en.cosel.co.jp/tool/tag/pdf/SFE_CHS.pdf (accessed October 2022).
- 18 COSEL Instruction Manual: https://en.cosel.co.jp/tool/tag/pdf/CME_CHS.pdf (accessed October 2022).
- 19 COSEL Applications manual for CHS series: https://en.cosel.co.jp/tool/tag/pdf/CHS_manual.pdf (accessed October 2022).
- 20 Delta Electronics Technical Specification Delphi Series V48SH, 1/16th Brick 100W. DC/DC Power Modules: https://filecenter.deltaww.com/products/download/01/0102/datasheet/DS_V48SH05020.pdf (accessed October 2022).
- 21 Murata Manufacturing Co., Ltd. Technical Specification ULS 100-Watt Series: <https://www.murata.com/zh-cn/products/productdata/8807040221214/ULS-100.pdf?1701142315000> (accessed October 2022).